
Geometry Guided Self-Consistency for Physical AI

Yinwei Dai Zhuofu Chen Lijie Yang Ravi Netravali
Princeton University
{yinweid,zhuofuc,ly322,rnetravali}@princeton.edu

Abstract

State-of-the-art physical AI models generate a chunk of actions per inference through diffusion or flow matching, iteratively refining an initial noise sample into an action trajectory. Because this inference process is inherently stochastic, committing to a single trajectory per round is brittle, and this brittleness compounds across the many sequential rounds that comprise a complete episode. We introduce KeyStone, an inference-time self-consistency method for diffusion-based action generation that draws K candidate action chunks in parallel from a shared model context, clusters them in continuous action space, and returns the medoid of the largest cluster – no additional model required. Two properties make this practical. First, the compact nature of action trajectories makes diffusion inference memory-bandwidth bound, leaving spare compute capacity to run K chains in parallel with no additional wall-clock latency. Second, unlike token or pixel spaces where distance carries no semantic meaning and selection requires a learned judge, action chunks are geometrically structured such that Euclidean distance directly reflects physical similarity, making selection principled and judge-free. Across diverse vision-language-action models (VLAs) and world-action models (WAMs), KeyStone improves task success rates by up to **13.3%** over single-trajectory sampling with negligible latency overhead, while having on par accuracy with model-based selectors at no training cost. We open source KeyStone at <https://github.com/dywsjtu/keystone>.

1 Introduction

Diffusion and flow-matching models have become the dominant paradigm for action generation in physical AI. They power vision-language-action models (VLAs) [Chi et al., 2024, Intelligence et al., 2025, NVIDIA et al., 2025, Shukor et al., 2025, Zheng et al., 2025] as well as world-action models (WAM) [Yuan et al., 2026, Ye et al., 2026, Kim et al., 2026] that couple action generations with a future-observation prediction. Across this family, the action generation paradigm is the same: at each call, the model denoises an initial noise sample into a *chunk* of actions, which is then executed open-loop on the robot before the model is queried again for the next chunk. This design captures the multimodal action distributions inherent in manipulation tasks and produces a smooth, temporally coherent control over continuous action spaces. A complete physical AI task, therefore, consists of many sequential rounds of action chunk sampling and execution.

This sampling-and-execution loop, however, is inherently stochastic. At each round, the policy starts from a fresh noise sample and iteratively refines it into an action chunk; different initial noises lead to different chunks, and not all of them succeed. Some fall into *failure regions* of the action space—chunks that, when executed, derail the task even when prior rounds were successful (Fig. 1b). Worse, this brittleness compounds: an episode comprises many rounds of chunk sampling (Fig. 1a), so even a small per-round probability of landing in a failure region accumulates into a substantial episode-level failure rate. Committing to a single sample per round, the standard practice today, leaves task success at the mercy of sampling noise.

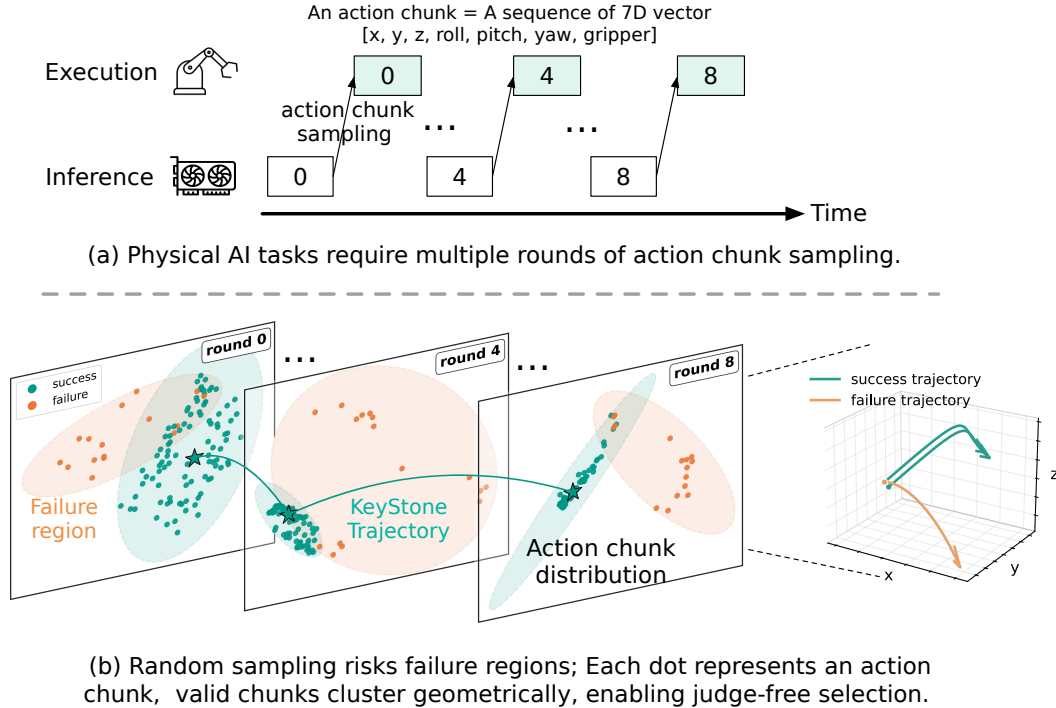


Figure 1: **Brittleness of single-trajectory sampling in physical AI.** (a) A complete episode consists of many rounds of action chunk sampling and open-loop execution. Each round’s stochastic sampling can derail the task. (b) At each round k , we draw many candidate chunks from GR00T N1.6 [NVIDIA et al., 2025] on SIMPLER [Li et al., 2024], execute each to episode end, and label the outcome **success** or **failure** (chunks are projected via per-round PCA). **success** chunks cluster densely while **failure** ones scatter. The inset shows the corresponding end-effector paths in 3D: **success** chunks lead to closer 3D trajectories that reach the goal, while a **failure** one clearly diverges. KeyStone exploits this by sampling multiple action chunks and selecting the medoid of the largest cluster at each round (**green stars**); chained together, these selections form the *KeyStone trajectory*.

A natural response to sampling stochasticity is test-time scaling: draw multiple candidates and select (e.g., self-consistency [Wang et al., 2023]), as studied extensively in language models [Wang et al., 2023, Cobbe et al., 2021, Lightman et al., 2023]. Recent work brings this paradigm to physical AI [Kwok et al., 2025, Yang et al., 2025], sampling multiple action candidates and selecting among them with a learned selector trained on the physical AI model’s fine-tuning dataset to score how well a candidate matches the in-distribution success modes. This adds non-trivial costs: an extra model to train per task and embodiment (hundreds of H100 hours in TACO Yang et al. [2025] for $\pi_{0.5}$ on LIBERO Liu et al. [2023], which exceeds $\pi_{0.5}$ ’s fine-tuning itself), plus an extra forward pass per round at inference.

Our key observation is that the geometry of sampled action chunks is surprisingly powerful: it directly encodes the model’s concentration on in-distribution behaviors, making the overheads associated with explicit learned selectors largely unwarranted. Action chunks live in a continuous space whose structure is constrained – every action is bounded by the robot’s physical degrees of freedom – so the Euclidean distance between two action chunks directly reflects whether they would drive the robot to similar execution trajectories. Unlike token or pixel spaces where Euclidean distance carries no semantic meaning (necessitating judges to bridge the gap), action spaces are physically constrained and low-dimensional, making distance a direct proxy for behavioral similarity. The model’s concentration on in-distribution behaviors therefore manifests directly as a dense cluster of geometrically proximate candidates; Fig. 1b shows this structure empirically.

Capitalizing on these insights, we present **KeyStone**, an inference-time self-consistency method that, at each round, draws K candidate action chunks in parallel from a single shared context, clusters them in the continuous action space, and returns the medoid of the largest cluster as the chunk to

execute. Importantly, because diffusion inference for action generation is memory-bandwidth bound, KeyStone’s parallel sampling fits within spare compute capacity and adds no additional wall-clock latency per round. This is because, unlike image and video diffusion, where the diffusion processes are compute-bound due to the large input dimensions, action diffusion operates over compact trajectories (typically $O(100)$ dimensions), shifting the bottleneck from compute to memory bandwidth and leaving substantial parallel compute headroom unused.

We evaluate across diverse VLAs and WAMs, and workloads, setting K to the largest value that preserves per-round latency, and find that KeyStone improves task success rates by up to **13.3%** over single-trajectory sampling and is comparable with the model-based test-time scaling approach TACO at zero training cost. More broadly, KeyStone shows that physical AI models inherently possess everything needed for successful self-consistency: the geometry to select without a judge, and the compute headroom to sample without added latency.

2 Background and Related Work

Action generation via diffusion and flow matching. Physical AI models map observational inputs—camera images, robot states, task instructions—to actions, low-level motor commands such as gripper signals or joint positions. To meet real-time constraints, state-of-the-art models output *action chunks*, or short sequences of future actions generated by iteratively refining an initial noise sample via diffusion or flow matching. This paradigm underlies VLAs such as π_0 [Intelligence et al., 2025], GR00T [NVIDIA et al., 2025], and SmolVLA [Shukor et al., 2025], as well as world-action models (WAMs) such as FastWAM [Yuan et al., 2026], Cosmos [Kim et al., 2026], and DreamZero [Ye et al., 2026], which additionally predict future observations such as video frames.

Test-time scaling in text and image generation. Sampling multiple candidates and selecting among them is a well-established way to improve generative model outputs. *Model-free* approaches avoid any auxiliary scorer: they select among candidates using a property of the candidates themselves, such as exact-match agreement on discrete final answers [Wang et al., 2023] or the model’s own output confidence [Fu et al., 2025]. *Model-based* approaches train a separate scorer when no such property is available—verifiers and process reward models [Cobbe et al., 2021, Lightman et al., 2023] for reasoning, and for image generation [Xu et al., 2023, Kirstain et al., 2023, Ma et al., 2025].

Test-time scaling in action generation. Earlier work extended test-time scaling to autoregressive VLAs. RoboMonkey [Kwok et al., 2025] samples K action candidates and selects with a VLM-based verifier; V-GPS [Nakamoto et al., 2025] trains a value function for the same purpose; MG-Select [Jang et al., 2025] scores candidates model-free via KL divergence from a condition-masked reference distribution. As physical AI has shifted toward diffusion- and flow-matching architectures, recent work has adapted selection to this paradigm. TACO [Yang et al., 2025] trains a pseudo-count estimator on the finetuning data and selects the candidate with the highest estimated count, constraining outputs to the finetuning data distribution. However, the auxiliary estimator adds inference overhead and must be retrained from the finetuning data and model-internal features at a cost of **hundreds of H100 hours** per task or embodiment—prohibitive given how often physical AI models are finetuned. The existing model-free direction does not transfer either: methods such as MG-Select rely on token-level confidence signals that an autoregressive model exposes natively from its final classifier, which diffusion- and flow-matching models lack. KDPE [Rosasco et al., 2025] applies kernel density estimation to the **final action** of N independent action chunks without a learned model. However, this does not scale to the dimensionality of full action chunks, forcing selection based on a single action point and discarding geometric signal across the rest of the chunk. KDPE also requires a task-specific manifold-aware kernel for each action representation. KeyStone instead exploits the general geometric structure of continuous action spaces to cluster over complete action chunks without task specific design, capturing richer signal across the full chunk. Overall, KeyStone is, to our knowledge, the first latency-neutral, judge-free test-time scaling method for diffusion- and flow-matching VLAs and WAMs, grounded in the geometric structure of continuous action spaces.

3 KeyStone

We introduce KeyStone, a drop-in inference-time wrapper for stochastic diffusion- and flow-matching physical AI models. At each round of the standard sample-and-execute loop, KeyStone draws multiple action chunks from the same encoded observations (e.g., camera images and robot states) and task instruction, identifies the largest cluster in continuous action space, and executes that cluster’s medoid – a real sampled chunk rather than a synthesized average. The method is therefore model-free: it uses only the geometry of the sampled action chunks, rather than a learned or task-specific selector.

3.1 Method Overview

Let c_t denote the encoded context at round t , including the task instruction, camera observations, and robot state. A diffusion- or flow-matching model maps this context and an initial noise tensor ϵ to an action chunk:

$$a = G_\theta(c_t, \epsilon), \quad \epsilon \sim \mathcal{N}(0, I), \tag{1}$$

where a is the sequence of future actions that will be executed sequentially before the next model call. Standard deployment draws one ϵ and commits to the resulting chunk. KeyStone instead draws K independent noises $\{\epsilon_i\}_{i=1}^K$ under the same context and obtains

$$a_i = G_\theta(c_t, \epsilon_i), \quad i = 1, \dots, K. \tag{2}$$

It then chooses one candidate $a^* \in \{a_i\}_{i=1}^K$ to execute. We return an actual generated action chunk, rather than an averaged trajectory, so the output remains on the model’s sampled action manifold and does not interpolate between distinct modes.

3.2 Latency-Preserving Parallel Sampling

The key efficiency insight is that K parallel chains can add no wall-clock latency when the dominant inference cost is context computation, because that context is shared across all candidates. Action diffusion operates over compact trajectories rather than large image or video latents, so the denoising computation is small and memory-bandwidth bound. This leaves free compute headroom for parallel sampling: once the shared prefix has been computed, adding candidates mainly adds small action-state tensors and batched denoising or flow updates.

Candidates share the same conditioning context. For VLAs, the image and language inputs are identical across candidates, so KeyStone computes the vision language model prefix once and reuses the resulting features or the transformer key-value (KV) cache for all K denoising chains. For WAMs, the same idea applies. The observation is passed through the video generation backbone once to produce the shared latent world embeddings. In implementation, this is a logical batch expansion: shared prefix feature tensors are first given a candidate dimension and expanded with `torch.expand`, so the K candidates share the same underlying storage rather than materializing K copies of the context. At each denoising or flow update step, the model processes those K candidates as a single batched forward pass. In practice, we choose K by profiling the target model on the deployment hardware and use the largest value whose per-round latency matches single-sample inference. We discuss the implementation details in the appendix.

3.3 Candidate Selection

The core insight behind our selector is that action chunks are ordered sequences of bounded robot commands. Nearby chunks in continuous action space correspond to physically similar execution trajectories by construction, so the largest dense region provides a natural model-free notion of consensus. KeyStone therefore clusters the sampled chunks in action space and executes the medoid rather than the centroid of the dominant cluster. This guarantees that the selected action is a real model output, avoiding interpolation between distinct modes that could produce trajectories that are physically invalid and inconsistent with the model’s output distribution.

To achieve that, each candidate chunk is first flattened into a vector x_i , and all pairwise L2 distances are computed in one batched tensor operation:

$$\Delta_{ij} = \|x_i - x_j\|_2. \tag{3}$$

Before clustering, KeyStone first checks whether clustering is needed. This guard handles a simple failure mode of forced clustering: when the candidate distribution is already unimodal, k-means can split one valid cluster into arbitrary halves, causing the selector to return the medoid of an artificial subcluster rather than the global medoid. To avoid this, KeyStone computes the global medoid $m = \arg \min_i \sum_j \Delta_{ij}$ and measures how far the sample mean \bar{x} lies from that medoid, normalized by the median pairwise distance:

$$s = \frac{\|\bar{x} - x_m\|_2}{\text{median}_{i < j} \Delta_{ij} + \epsilon}. \quad (4)$$

If s is below a threshold τ (default 0.3), the candidates are treated as a single compact cluster and KeyStone returns the global medoid a_m . The threshold is intentionally conservative: it only suppresses clustering when the mean and medoid nearly agree relative to the typical candidate spread, which is the regime where a cluster split is least informative. Otherwise, KeyStone runs cluster-medoid selection. The number of clusters is exposed as a hyperparameter C ; we use $C = 2$ by default because most manipulation decisions have one dominant valid mode and scattered failure samples, so the main decision is whether a candidate belongs to the consensus mode or not. Given C , KeyStone runs a small k-means loop over the flattened candidate chunks. We initialize the centroids by randomly selecting C candidates from the sampled batch. We iterate up to 10 times and stop early when the cluster assignments do not change between successive iterations. This assigns each candidate to a cluster,

$$z_i \in \{1, \dots, C\}, \quad \mathcal{C}_c = \{i : z_i = c\}. \quad (5)$$

It then chooses the largest cluster and returns that cluster’s medoid:

$$c^* = \arg \max_{c \in \{1, \dots, C\}} |\mathcal{C}_c|, \quad \mathcal{C}^* = \mathcal{C}_{c^*}, \quad i^* = \arg \min_{i \in \mathcal{C}^*} \sum_{j \in \mathcal{C}^*} \Delta_{ij}, \quad a^* = a_{i^*}. \quad (6)$$

The selected chunk is thus both representative of the dominant sampled mode and **guaranteed to be one of the model’s own outputs**. The rule has no trained parameters, no auxiliary scorer. Its cost is small for the sample counts used in our evaluations (<16): the filter uses the pairwise distances already computed for medoid selection, k-means runs over only K compact action chunks, and the within-cluster medoid reuses the same pair-wise distance matrix.

3.4 Deployment Loop

At deployment, KeyStone is a lightweight wrapper around the original policy sampler. At each round it intercepts the generation call, runs the parallel sampling and selection procedures of Sections 3.2–3.3, and returns a single action chunk to the downstream robotic application in the original output format. The selection step itself adds negligible overhead: its pairwise distances, k-means, and medoid arg-mins are all batched tensor operations over only K compact action chunks. We describe the implementation details in the appendix.

4 Evaluation

We evaluate KeyStone along the two axes implied by its design: whether parallel candidate sampling preserves wall-clock latency, and whether KeyStone’s candidate selection improves task success over the single-sample baseline while matching model-based test-time scaling approach TACO.

4.1 Experimental Setup

Testbed. We implement KeyStone as an inference wrapper across three evaluation testbeds: LeRobot [Cadene et al., 2026], vla-eval [Choi et al., 2026], and Fast-WAM [Yuan et al., 2026]. In each testbed, the $K = 1$ baseline is the original model evaluated under the configuration used to reproduce its reported behavior, including the benchmark suite, action chunk size, action post-processing, and per-task repeat episode count. For vla-eval, we use its benchmark Docker images so the simulator, dependencies, and other setups exactly match the original baseline setup. The baseline path is unchanged when the wrapper is disabled or when $K = 1$. For $K > 1$, the wrapper intercepts action generation, constructs a candidate batch from independent noise samples. The selector returns one selected action chunk, and the testbed passes that chunk through the same downstream execution path used by the baseline. We run our evaluations on NVIDIA A6000-48GB GPUs.

Models. Across these three testbeds, we evaluate KeyStone on physical AI models spanning VLAs and WAMs, including $\pi_{0.5}$ [Intelligence et al., 2025], SmolVLA [Shukor et al., 2025], GR00T N1.6 [NVIDIA et al., 2025], X-VLA [Zheng et al., 2025], StarVLA (Qwen VLM + GR00T action diffuser) [Community, 2026], and Fast-WAM [Yuan et al., 2026].

Workloads. We use simulated manipulation workloads from LIBERO [Liu et al., 2023], SimplerEnv [Li et al., 2024], and RoboTwin 2.0 [Chen et al., 2025]. For SimplerEnv, we evaluate both supported robot embodiments used in our results: WidowX and Google Robot. The workloads span single-arm tabletop manipulation, long-horizon instruction following, cross-embodiment settings, and dual-arm manipulation.

Metrics. Our primary metric is task success rate. Within each workload, every task is evaluated over the same number of episodes used by the baseline configuration in their papers or implementations, typically 24–100 episodes per task mentioned above. Each episode is one independent closed-loop rollout: the testbed instantiates the simulator from one of the task’s initial conditions (object poses, target configurations, scene seeds), executes the model in closed loop until the task succeeds or a fixed step budget is reached, and records a binary success label using the task’s success criterion. The per-task success rate is the fraction of these episodes that succeed, and the workload-level success rate reported in our tables is the average of the per-task rates within the workload. For each model–workload pair, we repeat this full evaluation five times unless otherwise noted—each repeat re-samples the per-episode sampling noise—and report the mean and one-standard-deviation range across the five repeats. The reported standard deviation therefore captures only the *across-repeat variation*; within-repeat noise is already absorbed into each repeat’s per-task success rate. We also report end-to-end per-round latency, which includes model inference for sampling the K candidates and final selection, and peak GPU memory during the same action-generation round.

4.2 Latency and Overhead

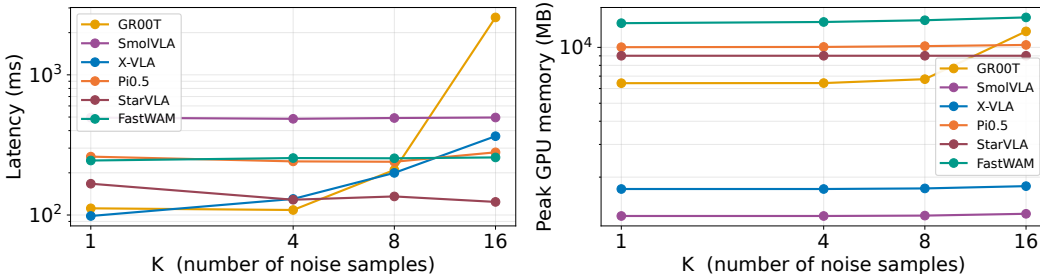


Figure 2: **End-to-end per-round latency and peak GPU memory as the number of sampled action chunks increases.** We measure the wall-clock latency of one action-generation round at $K \in \{1, 4, 8, 16\}$, including model inference, the overhead of sampling K candidates, and KeyStone’s selection step. We also report the peak GPU memory used by the same generation round.

Figure 2 reports KeyStone’s end-to-end latency and peak GPU memory as the number of sampled candidates K increases. The latency measurement includes model inference, parallel candidate sampling, and the cluster-based selection step. Drawing multiple candidate chunks in parallel adds little latency over the operating range used in our evaluations. Peak GPU memory also remains stable across these K values. This scaling comes from two properties. First, the shared model context is encoded and stored in memory once per round rather than once per candidate. Second, the per-candidate diffusion computation operates on compact action chunks. This compact action representation makes the diffusion process memory-bandwidth bound, leaving compute headroom for parallel candidate sampling without increasing latency. It also keeps the added activations and candidate-selection state small, adding little GPU memory overhead.

We therefore choose the largest K whose end-to-end latency remains close to the $K = 1$ baseline. For GR00T and X-VLA, latency begins to inflate beyond $K = 4$, so we use $K = 4$ in the subsequent evaluation. For the remaining models, we set $K = 16$ as the latency stays close to the baseline. These measurements assume the common single-robot deployment setting with a dedicated GPU; Section 5

Table 1: **Aggregate task success rates (%) on simulated manipulation workloads.** Mean \pm one standard deviation across 5 runs, where each run is macro-averaged across the tasks within each workload. Δ is the absolute (percentage-point) improvement of KeyStone over the $K=1$ baseline.

Workload	Model	K	Baseline ($K=1$)	KeyStone	Δ
LIBERO	$\pi_{0.5}$	16	96.8 ± 0.7	97.8 ± 1.1	+1.0
LIBERO	SmolVLA	16	50.4 ± 2.1	57.2 ± 1.3	+6.8
SimplerEnv – WidowX	GR00T N1.6	4	50.0 ± 4.3	63.3 ± 2.9	+13.3
SimplerEnv – WidowX	X-VLA	4	92.7 ± 1.0	95.8 ± 1.0	+3.1
SimplerEnv – WidowX	StarVLA	16	52.8 ± 1.6	59.7 ± 1.3	+6.9
SimplerEnv – Google Robot	GR00T N1.6	4	79.4 ± 3.5	86.7 ± 1.5	+7.3
Robotwin 2.0	Fast-WAM	16	90.0 ± 1.5	93.0 ± 1.0	+3.0

discusses the shared-accelerator case where the spare compute headroom that KeyStone’s parallel sampling relies on may shrink, and K should be re-profiled against the actual deployment workload.

4.3 Task Success Rates

Table 1 reports the workload-level success rate—computed as described in Section 4.1—for every model–workload pair, comparing the $K=1$ baseline against KeyStone at the per-model K chosen in Section 4.2 ($K=4$ for GR00T N1.6 and X-VLA, $K=16$ for the rest). Bold marks the higher mean per row, and the Δ column gives the absolute success rate improvement of KeyStone over the baseline.

KeyStone improves every model–workload pair, with absolute gains of +1.0 to +13.3 percentage points over the single-sample baseline. The improvements hold across both VLAs and the WAM, and across LIBERO, SimplerEnv on WidowX and Google Robot, and RoboTwin 2.0. The improvements appear on two axes—a higher mean success rate and a smaller across-repeat standard deviation—both arising from KeyStone’s better per-round sampling. We describe each effect in turn, then characterize the (model, workload) regime in which the gains concentrate.

Mean improvement. At each action-generation round, KeyStone selects the action chunk from the dominant sampled cluster rather than committing to a single stochastic draw, replacing the per-round failure rate of a generic random sample with that of the model’s dominant sampled mode. Because each rollout consists of many rounds, this per-round reduction compounds into the task-level success-rate gains in Table 1. Every row improves; the largest gain is +13.3 for GR00T N1.6 on SimplerEnv–WidowX (50.0% \rightarrow 63.3%). The gain on Fast-WAM (+3.0) confirms that KeyStone’s geometric selection generalizes beyond VLAs to WAMs, where the same geometric structure holds.

Variance reduction. The same mechanism also reduces the across-repeat standard deviation of the success rate. KeyStone consistently selects from the dominant cluster across rounds, so successive evaluations yield more similar task-level outcomes. The standard deviation drops from 4.3 to 2.9 for GR00T N1.6 on SimplerEnv–WidowX, from 3.5 to 1.5 on SimplerEnv–Google Robot, from 2.1 to 1.3 for SmolVLA on LIBERO, and from 1.6 to 1.3 for StarVLA on SimplerEnv–WidowX.

Region of benefit: high-variance baselines. KeyStone delivers its largest gains on workloads where the $K=1$ baseline shows visibly high across-repeat variance, the direct signature of a model whose single-sample inference is suffering from sampling randomness. The four rows with the highest $K=1$ standard deviations are exactly the four with the largest mean gains: GR00T N1.6 on SimplerEnv–WidowX (± 4.3 , $\Delta = +13.3$), GR00T N1.6 on SimplerEnv–Google Robot (± 3.5 , $\Delta = +7.3$), SmolVLA on LIBERO (± 2.1 , $\Delta = +6.8$), and StarVLA on SimplerEnv–WidowX (± 1.6 , $\Delta = +6.9$). All four also receive a meaningful variance reduction. The mechanism is consistent: workloads where single-sample inference visibly scatters across repeats are exactly the workloads where KeyStone has the most scattered failure samples to suppress, so suppressing them lifts the mean and tightens the spread together.

Where the gains plateau. At the opposite end, the rows where the $K=1$ baseline already operates with low variance and near-perfect accuracy give KeyStone no scattered failure mass to remove. $\pi_{0.5}$ on LIBERO, X-VLA on SimplerEnv–WidowX, and Fast-WAM on RoboTwin 2.0 all sit above 90%

Table 2: **Breakdown on LIBERO with $\pi_{0.5}$ ($K=16$).** Every suite (each has 10 tasks) is already saturated at $K=1$, so KeyStone contributes only small deltas that average to a +1.0 overall gain.

Suite	Baseline ($K=1$)	KeyStone	Δ
Spatial	96.0 \pm 1.4	98.0 \pm 1.4	+2.0
Object	99.0 \pm 1.4	99.5 \pm 0.7	+0.5
Goal	98.0 \pm 1.4	97.5 \pm 0.7	-0.5
Long	94.0 \pm 1.4	95.0 \pm 1.4	+1.0
Overall	96.8 \pm 0.7	97.8 \pm 1.1	+1.0

Table 3: **Breakdown on SimplerEnv–WidowX with X-VLA ($K=4$).** Two tasks are already saturated at $K=1$ ($\geq 98\%$); the overall +3.1 gain comes mostly from the improvement on the two less-saturated tasks.

Task	Baseline ($K=1$)	KeyStone	Δ
Put Carrot on Plate	100.0 \pm 0.0	100.0 \pm 0.0	0.0
Put Eggplant in Basket	88.9 \pm 6.4	95.8 \pm 4.2	+6.9
Put Spoon on Tablecloth	98.6 \pm 2.4	100.0 \pm 0.0	+1.4
Stack Green Cube	83.3 \pm 4.2	87.5 \pm 1.6	+4.2
Overall	92.7 \pm 1.0	95.8 \pm 1.0	+3.1

at $K=1$ with $K=1$ standard deviations of 1.5 or less, and the corresponding gains are modest (+1.0, +3.1, +3.0). Table 2 drills into the $\pi_{0.5}$ on LIBERO case: every one of the four LIBERO suites (each has 10 tasks) is already at or above 94% at $K=1$, so KeyStone contributes only small per-suite deltas (ranging from -0.5 to $+2.0$) that average to a +1.0 macro gain. Table 3 shows the X-VLA on SimplerEnv–WidowX case, which is more heterogeneous: two of the four tasks are already at or above 98% at $K=1$ and contribute essentially nothing, while the two less-saturated tasks (Eggplant in Basket at 88.9%, Stack Green Cube at 83.3%) improve by 6.9% and 4.2% respectively, averaging to a 3.1% macro gain. This regime is where KeyStone’s benefit asymptotes: saturated baselines with high success rates and low variance directly implies that the model is already concentrating on the dominant mode, leaving consensus selection nothing distinct to recover. Symmetrically, KeyStone’s benefit also vanishes at the opposite end of the spectrum—models where the majority of samples are confidently wrong, in which case cluster-medoid selection picks from the incorrect dominant cluster—since KeyStone only selects among the sampled candidates and cannot produce a successful chunk if none would succeed; we treat this as an assumption and discuss it in Section 5.

Table 4: **Comparison with TACO on RoboTwin 2.0 with $\pi_{0.5}$.** Each task is evaluated 50 times.

Task	Baseline ($K=1$)	TACO	KeyStone
Adjust Bottle	88.0%	94.0%	92.0%
Beat Block Hammer	68.0%	66.0%	70.0%
Handover Block	24.0%	30.0%	34.0%
Move Can Pot	42.0%	60.0%	54.0%
Place Object Stand	68.0%	80.0%	72.0%
Overall	58.0%	66.0%	64.4%

Comparison with TACO. On the five RoboTwin 2.0 tasks for which TACO [Yang et al., 2025] has released trained selectors, KeyStone matches TACO at the macro level (64.4% vs 66.0%, both at $K=16$ over a 58.0% $K=1$ baseline; Table 4). It does so without TACO’s per-task auxiliary training (hundreds of GPU hours), demonstrating that action-chunk geometry alone is a powerful selection signal to match model based approaches.

4.4 Ablations

We ablate three components of KeyStone’s selector: the distance function, the number of samples K , and the number of clusters C . To control evaluation cost we run ablations on the five vla-eval pairs in

Table 1; each ablation varies one component while holding the rest at their defaults (L2 distance, K from Section 4.2, $C=2$). Table 5 reports the resulting per-pair improvement over the $K=1$ baseline.

Table 5: **Ablations on KeyStone’s selector.** Each cell is the absolute (percentage-point) improvement over the $K=1$ baseline. *Default:* L2 distance, $C=2$, and K chosen as in Section 4.2 ($K=4$ for GR00T N1.6 and X-VLA, $K=16$ otherwise). The ablation columns vary one component at a time. Bold marks the largest gain per column.

Workload	Model	Default	Cosine	2K	C=4
LIBERO	$\pi_{0.5}$	+1.0	+0.3	+1.7	+1.1
SimplerEnv – WidowX	GR00T N1.6	+13.3	+0.5	+14.2	+8.3
SimplerEnv – WidowX	X-VLA	+3.1	+1.7	+2.7	+1.4
SimplerEnv – WidowX	StarVLA	+6.9	+3.1	+7.5	+5.9
SimplerEnv – Google Robot	GR00T N1.6	+7.3	+5.0	+6.8	+6.2

L2 vs cosine. Cosine distance reduces the gain on every pair, most dramatically on GR00T N1.6/WidowX (+0.5 vs +13.3 for L2). Action chunks are bounded physical commands whose magnitude is meaningful, so a magnitude-blind metric loses the structure cluster-medoid relies on (Section 3.3).

Number of samples: K vs $2K$. Doubling K produces only small fluctuations around the default, indicating that the chosen K is already near the saturation point of mode estimation. K therefore serves as a tunable knob for trading off latency and accuracy: our chosen values sit near the accuracy saturation point while preserving the latency, and operators can dial K up for higher and more stable accuracy with higher latency overheads.

Number of clusters: $C=2$ vs $C=4$. Increasing C from 2 to 4 produces comparable or smaller gains on every pair. The default $C=2$ matches the structure we observe in our workloads often have a single dominant mode plus scattered failure samples. Therefore, additional clusters risk splitting the dominant mode itself.

5 Limitations

Like other existing test-time scaling methods for both language models and physical AI models, KeyStone assumes that the underlying model is properly trained and samples useful candidate trajectories. It can choose a better action chunk among the sampled candidates, but it cannot produce a successful action if none of the sampled candidates would succeed, or if the model is confidently wrong on the majority of samples—in that case cluster-medoid selection picks from the incorrect dominant cluster and may even amplify the error rather than suppress it. Additionally, our latency measurements use batch size one, a common robot-deployment setting with a dedicated GPU. When the same accelerator is shared across multiple robots and the effective batch size is already large, the available headroom for additional parallel samples may shrink; in such cases, K should be chosen by profiling the deployment workload.

6 Conclusion

Diffusion- and flow-matching physical AI models are powerful, but their standard deployment loop still commits to one stochastic action chunk at each round. KeyStone addresses this brittleness with a simple inference-time wrapper: sample several chunks from the same context, use the geometry of continuous action space to find the dominant consensus mode, and execute that mode’s medoid as a real model output. This enables judge-free self-consistency for action generation. Two properties make KeyStone effective and practical. First, action chunks are compact, so parallel sampling can reuse the shared model context and add little end-to-end latency. Second, the geometry of output action chunks provides a natural signal for model confidence. Across VLA and WAM testbeds, KeyStone improves task success over single-trajectory sampling by up to 13.3%, while remaining on par with model-based test-time scaling approaches. More broadly, KeyStone shows that test-time scaling for physical AI can be grounded with the geometry structure of the model’s own output.

References

- Remi Cadene, Simon Aliberts, Francesco Capuano, Michel Aractingi, Adil Zouitine, Pepijn Kooijmans, Jade Choghari, Martino Russi, Caroline Pascal, Steven Palma, Mustafa Shukor, Jess Moss, Alexander Soare, Dana Aubakirova, Quentin Lhoest, Quentin Gallouédec, and Thomas Wolf. Lerobot: An open-source library for end-to-end robot learning, 2026. URL <https://arxiv.org/abs/2602.22818>.
- Tianxing Chen, Zanxin Chen, Baijun Chen, Zijian Cai, Yibin Liu, Zixuan Li, Qiwei Liang, Xianliang Lin, Yiheng Ge, Zhenyu Gu, Weiliang Deng, Yubin Guo, Tian Nian, Xuanbing Xie, Qiangyu Chen, Kailun Su, Tianling Xu, Guodong Liu, Mengkang Hu, Huan ang Gao, Kaixuan Wang, Zhixuan Liang, Yusen Qin, Xiaokang Yang, Ping Luo, and Yao Mu. Robotwin 2.0: A scalable data generator and benchmark with strong domain randomization for robust bimanual robotic manipulation, 2025. URL <https://arxiv.org/abs/2506.18088>.
- Cheng Chi, Zhenjia Xu, Siyuan Feng, Eric Cousineau, Yilun Du, Benjamin Burchfiel, Russ Tedrake, and Shuran Song. Diffusion policy: Visuomotor policy learning via action diffusion, 2024. URL <https://arxiv.org/abs/2303.04137>.
- Suhwan Choi, Yunsung Lee, Yubeen Park, Chris Dongjoo Kim, Ranjay Krishna, Dieter Fox, and Youngjae Yu. vla-eval: A unified evaluation harness for vision-language-action models, 2026. URL <https://arxiv.org/abs/2603.13966>.
- Karl Cobbe, Vineet Kosaraju, Mohammad Bavarian, Mark Chen, Heewoo Jun, Lukasz Kaiser, Matthias Plappert, Jerry Tworek, Jacob Hilton, Reiichiro Nakano, Christopher Hesse, and John Schulman. Training verifiers to solve math word problems, 2021. URL <https://arxiv.org/abs/2110.14168>.
- StarVLA Community. Starvla: A lego-like codebase for vision-language-action model developing. *arXiv preprint arXiv:2604.05014*, 2026.
- Yichao Fu, Xuwei Wang, Yuandong Tian, and Jiawei Zhao. Deep think with confidence, 2025. URL <https://arxiv.org/abs/2508.15260>.
- Physical Intelligence, Kevin Black, Noah Brown, James Darpinian, Karan Dhabalia, Danny Driess, Adnan Esmail, Michael Equi, Chelsea Finn, Niccolo Fusai, Manuel Y. Galliker, Dibya Ghosh, Lachy Groom, Karol Hausman, Brian Ichter, Szymon Jakubczak, Tim Jones, Liyiming Ke, Devin LeBlanc, Sergey Levine, Adrian Li-Bell, Mohith Mothukuri, Suraj Nair, Karl Pertsch, Allen Z. Ren, Lucy Xiaoyang Shi, Laura Smith, Jost Tobias Springenberg, Kyle Stachowicz, James Tanner, Quan Vuong, Homer Walke, Anna Walling, Haohuan Wang, Lili Yu, and Ury Zhilinsky. $\pi_{0.5}$: a vision-language-action model with open-world generalization, 2025. URL <https://arxiv.org/abs/2504.16054>.
- Suhyeok Jang, Dongyoung Kim, Changyeon Kim, Youngsuk Kim, and Jinwoo Shin. Verifier-free test-time sampling for vision language action models, 2025. URL <https://arxiv.org/abs/2510.05681>.
- Moo Jin Kim, Yihuai Gao, Tsung-Yi Lin, Yen-Chen Lin, Yunhao Ge, Grace Lam, Percy Liang, Shuran Song, Ming-Yu Liu, Chelsea Finn, and Jinwei Gu. Cosmos policy: Fine-tuning video models for visuomotor control and planning, 2026. URL <https://arxiv.org/abs/2601.16163>.
- Yuval Kirstain, Adam Polyak, Uriel Singer, Shahbuland Matiana, Joe Penna, and Omer Levy. Pick-a-pic: An open dataset of user preferences for text-to-image generation, 2023. URL <https://arxiv.org/abs/2305.01569>.
- Jacky Kwok, Christopher Agia, Rohan Sinha, Matt Foutter, Shulu Li, Ion Stoica, Azalia Mirhoseini, and Marco Pavone. Robomonkey: Scaling test-time sampling and verification for vision-language-action models, 2025. URL <https://arxiv.org/abs/2506.17811>.
- Xuanlin Li, Kyle Hsu, Jiayuan Gu, Karl Pertsch, Oier Mees, Homer Rich Walke, Chuyuan Fu, Ishikaa Lunawat, Isabel Sieh, Sean Kirmani, Sergey Levine, Jiajun Wu, Chelsea Finn, Hao Su, Quan Vuong, and Ted Xiao. Evaluating real-world robot manipulation policies in simulation, 2024. URL <https://arxiv.org/abs/2405.05941>.

- Hunter Lightman, Vineet Kosaraju, Yura Burda, Harri Edwards, Bowen Baker, Teddy Lee, Jan Leike, John Schulman, Ilya Sutskever, and Karl Cobbe. Let’s verify step by step, 2023. URL <https://arxiv.org/abs/2305.20050>.
- Bo Liu, Yifeng Zhu, Chongkai Gao, Yihao Feng, Qiang Liu, Yuke Zhu, and Peter Stone. Libero: Benchmarking knowledge transfer for lifelong robot learning, 2023. URL <https://arxiv.org/abs/2306.03310>.
- Nanye Ma, Shangyuan Tong, Haolin Jia, Hexiang Hu, Yu-Chuan Su, Mingda Zhang, Xuan Yang, Yandong Li, Tommi Jaakkola, Xuhui Jia, and Saining Xie. Inference-time scaling for diffusion models beyond scaling denoising steps, 2025. URL <https://arxiv.org/abs/2501.09732>.
- Mitsuhiko Nakamoto, Oier Mees, Aviral Kumar, and Sergey Levine. Steering your generalists: Improving robotic foundation models via value guidance, 2025. URL <https://arxiv.org/abs/2410.13816>.
- NVIDIA, :, Johan Bjorck, Fernando Castañeda, Nikita Cherniadev, Xingye Da, Runyu Ding, Linxi "Jim" Fan, Yu Fang, Dieter Fox, Fengyuan Hu, Spencer Huang, Joel Jang, Zhenyu Jiang, Jan Kautz, Kaushil Kundalia, Lawrence Lao, Zhiqi Li, Zongyu Lin, Kevin Lin, Guilin Liu, Edith Llontop, Loic Magne, Ajay Mandlekar, Avnish Narayan, Soroush Nasiriany, Scott Reed, You Liang Tan, Guanzhi Wang, Zu Wang, Jing Wang, Qi Wang, Jiannan Xiang, Yuqi Xie, Yinzhen Xu, Zhenjia Xu, Seonghyeon Ye, Zhiding Yu, Ao Zhang, Hao Zhang, Yizhou Zhao, Ruijie Zheng, and Yuke Zhu. Gr00t n1: An open foundation model for generalist humanoid robots, 2025. URL <https://arxiv.org/abs/2503.14734>.
- Andrea Rosasco, Federico Ceola, Giulia Pasquale, and Lorenzo Natale. Kdpe: A kernel density estimation strategy for diffusion policy trajectory selection, 2025. URL <https://arxiv.org/abs/2508.10511>.
- Mustafa Shukor, Dana Aubakirova, Francesco Capuano, Pepijn Kooijmans, Steven Palma, Adil Zouitine, Michel Aractingi, Caroline Pascal, Martino Russi, Andres Marafioti, Simon Alibert, Matthieu Cord, Thomas Wolf, and Remi Cadene. Smolvla: A vision-language-action model for affordable and efficient robotics, 2025. URL <https://arxiv.org/abs/2506.01844>.
- Xuezhi Wang, Jason Wei, Dale Schuurmans, Quoc Le, Ed Chi, Sharan Narang, Aakanksha Chowdhery, and Denny Zhou. Self-consistency improves chain of thought reasoning in language models, 2023. URL <https://arxiv.org/abs/2203.11171>.
- Jiazheng Xu, Xiao Liu, Yuchen Wu, Yuxuan Tong, Qinkai Li, Ming Ding, Jie Tang, and Yuxiao Dong. Imagereward: Learning and evaluating human preferences for text-to-image generation, 2023. URL <https://arxiv.org/abs/2304.05977>.
- Siyuan Yang, Yang Zhang, Haoran He, Ling Pan, Xiu Li, Chenjia Bai, and Xuelong Li. Steering vision-language-action models as anti-exploration: A test-time scaling approach, 2025. URL <https://arxiv.org/abs/2512.02834>.
- Seonghyeon Ye, Yunhao Ge, Kaiyuan Zheng, Shenyuan Gao, Sihyun Yu, George Kurian, Suneel Indupuru, You Liang Tan, Chuning Zhu, Jiannan Xiang, Ayaan Malik, Kyungmin Lee, William Liang, Nadun Ranawaka, Jiasheng Gu, Yinzhen Xu, Guanzhi Wang, Fengyuan Hu, Avnish Narayan, Johan Bjorck, Jing Wang, Gwanghyun Kim, Dantong Niu, Ruijie Zheng, Yuqi Xie, Jimmy Wu, Qi Wang, Ryan Julian, Danfei Xu, Yilun Du, Yevgen Chebotar, Scott Reed, Jan Kautz, Yuke Zhu, Linxi "Jim" Fan, and Joel Jang. World action models are zero-shot policies, 2026. URL <https://arxiv.org/abs/2602.15922>.
- Tianyuan Yuan, Zibin Dong, Yicheng Liu, and Hang Zhao. Fast-wam: Do world action models need test-time future imagination?, 2026. URL <https://arxiv.org/abs/2603.16666>.
- Jinliang Zheng, Jianxiong Li, Zhihao Wang, Dongxiu Liu, Xirui Kang, Yuchun Feng, Yinan Zheng, Jiayin Zou, Yilun Chen, Jia Zeng, Ya-Qin Zhang, Jiangmiao Pang, Jingjing Liu, Tai Wang, and Xianyuan Zhan. X-vla: Soft-prompted transformer as scalable cross-embodiment vision-language-action model, 2025. URL <https://arxiv.org/abs/2510.10274>.

A Technical Appendices and Supplementary Material

A.1 Implementation: KeyStone as an Inference-Time Wrapper

KeyStone is implemented as a lightweight Python wrapper that intercepts each action-generation call of an existing policy and replaces it with K -sample parallel inference plus cluster-medoid selection. The wrapper does not modify model weights, retrain any component, or change the downstream control loop. Across the three testbeds we evaluate on (LeRobot, vla-eval, Fast-WAM), the integration follows the same three-step pattern at each round:

1. **Shared context expansion.** The current observations and task instruction are encoded once. The resulting prefix tensors (VLM features, transformer KV cache, or world embedding) are given a candidate dimension and expanded to width K via `torch.expand`, so that the K candidates share the same underlying storage rather than materializing K copies of the context.
2. **Batched candidate sampling.** We draw K independent noise tensors and run the model’s denoising or flow-matching loop as a single batched forward pass, producing K candidate action chunks $\{a_i\}_{i=1}^K$.
3. **Cluster-medoid selection.** Each candidate is flattened, the $K \times K$ pairwise L2 distance matrix is computed in one batched tensor operation, and the threshold-guarded cluster-medoid procedure of Section 3.3 returns a single action chunk a^* , which is handed to the existing controller in the original output format.

LeRobot. For policies using the LeRobot inference loop ($\pi_{0.5}$ and SmolVLA in our evaluation), we subclass each policy and override its action-generation method. The override replaces the original noise sampling and denoising/flow-matching steps with their batched (K -wide) versions, calls into the shared selector, and returns a single chunk in the original output format. The downstream LeRobot controller sees no change.

vla-eval. For policies served from vla-eval benchmark Docker images (GR00T N1.6, X-VLA, and StarVLA in our evaluation), we wrap the inference module inside each image. The wrapper reuses the image’s existing model loading, observation pre-processing, and action post-processing, and intercepts only the function that maps an encoded observation context to an action chunk. This keeps the simulator, dependencies, and hardware setup byte-identical to the reproduced baseline.

Fast-WAM. For the world-action model setting (Fast-WAM in our evaluation), we wrap the per-round generate step. The video generation backbone runs once per round to produce the shared world embedding; we expand the embedding to a K -batch and run the action decoder’s denoising loop as a single batched pass. The selector runs identically to the VLA case.

Selector implementation. The cluster-medoid selector is implemented in PyTorch as a small set of batched on-GPU operations: a $K \times K$ pairwise L2 distance matrix, a global-medoid argmin, the threshold- τ unimodality guard (with $\tau = 0.3$ as the default), a small k-means loop ($C=2$, up to 10 iterations) over the flattened action chunks, and a within-cluster medoid argmin. All steps reuse the precomputed distance matrix; the entire selection adds at most a few hundred microseconds per round at the K values used in our evaluation.

Listing 1 sketches the wrapper that intercepts an existing policy’s action-generation call, and Listing 2 shows the corresponding cluster-medoid selector.

Listing 1: **Wrapper integration pattern.** KeyStone subclasses an existing policy and replaces the per-round action call with shared-context expansion, batched K -sample generation, and cluster-medoid selection.

```
class KeyStonePolicy(BasePolicy):
    def __init__(self, base_policy, K=16, C=2, tau=0.3):
        self.base = base_policy
        self.K, self.C, self.tau = K, C, tau

    def predict_action(self, observation):
        # 1. Encode shared context once (VLM features, KV cache,
```

```

# or world embedding -- depends on the base policy).
context = self.base.encode(observation)

# 2. Expand to a K-batch *without* materializing K copies.
context_K = expand_to_K(context, self.K) # uses torch.expand

# 3. Run K denoising or flow chains as one batched forward.
noise = torch.randn(self.K, *self.base.noise_shape,
                    device=context.device)
candidates = self.base.sample_actions(context_K, noise)
# candidates: [K, T, action_dim]

# 4. Cluster-medoid selection -- returns one real chunk.
return cluster_medoid_select(candidates,
                            C=self.C, tau=self.tau)

```

Listing 2: **Cluster-medoid selector.** All steps are batched on-GPU and reuse the same pairwise distance matrix. τ guards against forced clustering of an already-unimodal candidate set (Section 3.3).

```

def cluster_medoid_select(actions, C=2, tau=0.3, eps=1e-8):
    # actions: [K, T, action_dim]
    X = actions.flatten(start_dim=1) # [K, D]
    K = X.shape[0]

    # Pairwise L2 distance matrix (reused throughout).
    dists = torch.cdist(X, X) # [K, K]

    # Global medoid (argmin of row sums of distances).
    m = dists.sum(dim=1).argmin() # scalar

    # Unimodality guard: how far is the mean from the medoid,
    # normalized by the typical pairwise distance?
    iu = torch.triu_indices(K, K, offset=1)
    median_d = dists[iu[0], iu[1]].median()
    s = (X.mean(dim=0) - X[m]).norm() / (median_d + eps)
    if s < tau:
        return actions[m] # already unimodal

    # Otherwise: k-means over K compact vectors, take the
    # largest cluster's medoid.
    z = kmeans(X, C=C, max_iter=10) # [K] cluster ids
    c_star = torch.bincount(z).argmax()
    mask = (z == c_star)
    sub_dists = dists[mask][:, mask]
    i_local = sub_dists.sum(dim=1).argmin()
    i_star = mask.nonzero(as_tuple=True)[0][i_local]
    return actions[i_star]

```